Final Technical Report

Name: Alemayehu L. Jemberie

Award No. 07HQGR0054

Region: Central and Eastern U.S.

Project Title: Study of Sediment Nonlinearity Using Explosion and Natural Earthquake Data.

Institution: Department of Physics, North Carolina A&T State University , 1601 East Market Street, Greensboro, NC 27411

Current address: Impact Forecasting, Aon Re Inc., 200 East Randolph Street, 20th Floor, Chicago, IL, 60601, e-mail: Alemayehu_Jemberie@aon.com, Tel: 312-381-5882, Fax: 312-381-0181

Publication: The following material is submitted to the **Journal of** "**Pure and Applied Geophysics**"

Study of Sediment Nonlinearity Using Explosion Data in the Mississippi Embayment

By Alemayehu Lakew Jemberie
Impact Forecasting, Aon Re Inc, 200 E. Randolph St., 20th floor, Chicago, IL, 60601
e-mail: Alemayehu_Jemberie@aon.com, Tel: 312-381-5882, Fax: 312-381-0181

Abstract

Strong- and weak- motion data from the Mississippi Embayment Seismic Excitation Experiment (ESEE) were analyzed for signatures of non-linear site responses. This experiment was performed jointly by the University of Memphis and US Geological survey in October 2002, by detonating two explosions of 2500 and 5000lbs. Intrinsic and scattering Q estimates (Q_I and Q_S) from the coda of the strong motion data were found to be very low compared to previously determined Q values of P- and Rayleigh-waves of weak motions data from the same explosions. The Q_I estimates from P-wave late coda of the strong motion data are less by more than a 100 at 3Hz and by more than 200 at 10Hz compared to the P-wave Q values determined from the weak motion data by Langston et al (2005). Also, Q_I determined from the late coda of strong motion Rayleigh-wave data is less by more than 200 at 0.5Hz and by more than 50 at 3.0Hz compared to Q values determined from Rayleigh-wave weak motion data. A resonance peak spectral amplitude of the early part of a strong motion seismogram is shifted to lower frequencies compared to that from a later part of the same seismogram. Spectral amplitude ratios between transverse and vertical components of the strong motion data are degraded below 6Hz compared to the weak motion transverse to vertical spectral ratio. All these are signatures of non-linear site responses during strong ground motion. This study proves the non-transportability of weak motion attenuation results to estimate ground motion

from a future large earthquake that may happen in areas like the New Madrid Seismic zone.

Key words: Mississippi Embayment, coda Q, nonlinear site response, intrinsic attenuation, scattering attenuation, strong motion data

Introduction

Nonlinearity is the name given to a range of physical manifestations that arise when strains associated with seismic waves become large enough that they affect the properties of the soil that determine wave propagation, particularly the wave speed and attenuation. It typically causes resonance frequency shifts and amplitude reduction. These phenomena are referred to as "Nonlinear Fast Dynamics" (NFD) by physicists (e.g., Johnson and Sutin, 2005), "modulus reduction" and "viscous" or "hysteretic damping" by geotechnical engineers (e.g., Hardin and Drnevich, 1972), and "seismic velocity changes" and "intrinsic attenuation" by seismologists (e.g., Beresnev et al., 1994). They have been observed during large natural earthquakes (e.g. the 1994 magnitude 6.7 NorthRidge earthquake [Field et al., 1998]; the 2001 M 6.8 Nisqually, Washington, earthquake [Frankel et al., 2002]). However, observing non-linearity in situ in regions where large earthquakes are uncommon (yet remain a major hazard) presents a difficult and important challenge. In this research, we investigate whether the same phenomena can be observed from strong motion data generated by artificial (explosive) seismic sources. In engineering lab experiments on Earth materials, viscous damping is calculated from an experimentally measured hysteretic stress-strain curve. The viscous

damping values obtained this way are interpreted by engineers as being due to the anelastic absorption of energy. However, the attenuation of seismic wave amplitudes also can arise from scattering (redistribution) of seismic energy by heterogeneities within the Earth. Intrinsic and scattering attenuation values can be obtained from coda of seismic waves (e.g., Jemberie and Langston, 2005). In this research we will see if both scattering and intrinsic attenuations change during strong motion from explosive sources; changes in intrinsic attenuation are expected for sediments that respond nonlinearly to strong shaking.

In October 2002, the Center for Earthquake Research and Information (CERI) at the University of Memphis and the U.S. Geological Survey performed an active source field experiment called the Embayment Seismic Excitation Experiment (ESEE; Langston et al., 2002). The experiment detonated two (2500lb and 5000lb) explosions in the Mississippi embayment (Figure 1) to study surface waves attenuation in the Embayment (Langston, 2005). The first, 2500lb, explosive was detonated on October 29, 2002 near Marked Tree, Arkansas, and the second, 5000lb, was detonated on October 30, 2002, near Mooring, TN. Arrays of 8 strong-motion seismographs were installed 2.5 km from the first explosion and 1.25 km from the second explosion with 15 meters inter-station spacing (Figure 1 for blast 1, and Langston et al., 2006). The ground motion reaches 2g near each blast. Broadband stations in the Mississippi embayment also recorded weak motions from these blasts. Investigation of both strong- and weak-motion data were undertaken to infer any non-linear site effects due to the sedimentary structure of the Mississippi embayment. The Mississippi embayment is a gentle synform in the central

United States filled with up to 2km of unconsolidated sediments (Stearns 1957; Stearns and Marcher, 1962; Self, 1993).

The goal of this paper is to better understand the nonlinear response to earthquakes' strong ground motion within thick unconsolidated sediments. While nonlinear ground motions are presumed to affect many places, there is a particular need to understand the processes that take place in the deep soils surrounding the New Madrid seismic zone in the Mississippi embayment of the central US.

Array data

The array data from the two explosions (data from blast 1 only is shown here) show distinct body wave and surface wave arrivals that propagate within the thick, unconsolidated sedimentary column, the high velocity basement rocks and small-scale structure near the surface (Figure 2; Langston et al., 2006). In Figure 2b, a large radial coda phase at about 16 sec for the first blast appears within the array and grows from nearly zero amplitude (at a distance of ~2.5 km) to values that almost saturate the instruments over the array length. This observation suggests that waves are being scattered by velocity heterogeneity in the embayment. These data were the highest amplitude strong motion data yet recorded in the Mississippi embayment (Langston et al., 2006). Vertical motions at the stations near each blast attained peak accelerations greater than 2 g and peak accelerations at the two arrays were roughly 20% g (Figure 4). The transverse component (Figure 2c), not expected from an axysymmetric explosion, is very strong and filled with scattered Rayleigh-waves (Langston et al., 2006).

Data from these arrays offer a unique opportunity to examine several important attributes of high frequency strong ground motion in the Mississippi embayment that are expected be useful to seismic engineering design since there are no comparable strong motion data from natural earthquakes in the area. We analyze the seismic waves recorded by stations deployed in ESEE to estimate intrinsic and scattering Q, resonance frequency shifts and amplitude reductions, which are key parameters describing nonlinear behavior.

Nonlinearity from explosion data in the Mississippi embayment

Nonlinearity has been observed in laboratory experiments on rocks at low frequency (~10^{-2} Hz) and large strains (~10^{-3}) values (quasi-static experiments; e.g. Johnson and Rasolofosaon, 1996) as well as at high frequency (~10^{4} Hz) and low strain (~10^{-8}) values (dynamic experiments; e.g. Johnson et al., 1996; Guyer et al., 1999; Ostrovsky and Johnson, 2001). Quasi-static experimental results show a hysteretic relationship between stress and strain. Dynamic experiments show signatures of nonlinearity, such as resonance frequency shifts towards lower values, and attenuation (nonlinear damping) as the applied pressure (driving level) increases. Engineering laboratory experiments on soils indicate a decrease in modulus and increase in viscous damping (attenuation) as strain increases (Schneider et al., 1999**)**. These nonlinear behaviors are also observed from seismological data. For example, strong motion and weak motion data from the 1994 magnitude 6.7 Northridge earthquake, and from the

2001 M 6.8 Nisqually, Washington, earthquake, indicated a decrease in the amplitude of the strong motion as well as a shift in the resonance frequency (Field et al., 1998; Frankel et al., 2002).

Langston et al (2005) analyzed weak motion data recorded by broad-band seismic stations from three explosions, including the two shown in Figure (1), to estimate Q values from P-wave (Q_P) and S-wave (Q_R, from Rayleigh-wave). The average Q_p and Q_R values found in their study are 200 and 100, respectively. The explosions are strong only near the approximately less than 3km array of strong motion sensors (Figure 11). The major, unanswered question is: Do strong ground motions from large earthquakes show similar attenuation (intrinsic and scattering) as weak motions? Will the damping, or intrinsic attenuation increase as predicted by nonlinear models? In seismic hazard assessment, attenuation values from weak motions are used to estimate the ground displacement from future large earthquakes. Are the attenuation values from weak motions transportable to estimations of amplitudes from strong ground motions?

One approach to looking for and studying nonlinear signatures during strong ground motion is to use explosion data. Analysis of the seismograms from explosions suggests that explosions' strong motion data may be used as a proxy for earthquakes' strong motion data (Langston et al. 2005). We try to answer the above questions by analyzing the strong motion data from the blast 1 shown in Figure 1.

CODA Q FROM STRONG MOTION DATA

Coda refers to the last arriving seismic waves, presumed to be waves that travel complex paths as they reflect off material heterogeneities. We obtain intrinsic and

scattering Q values from the P- and Rayleigh-wave coda of the recorded seismograms using the Energy Flux model (Frankel and Wennerberg, 1987; Langston, 1989 (a,b); Jemberie and Langston 2005,) and Aki's (Aki, 1969; Aki and Chouet, 1975) single scattering model.

For two-dimensional media, coda amplitude, Ac, is given by the energy-flux model as:

$$\mathrm{Ac} = \sqrt{2I_D}\, t_d^{\,1/2} t^{-1} e^{-\omega t/(2Q_I)} e^{\omega t_d (1/Q_I + 1/Q_S)/2} \sqrt{1 - e^{-\omega t/Q_S}} \,. \qquad (1)$$

Where I_d is the integral of the square of the direct wave seismogram amplitude. t_d and t are direct wave travel time and coda lapse time in seconds, respectively, measured from the earthquake origin time. Q_I is intrinsic Q and Q_S is scattering Q. ω is the angular frequency measured in rad/sec. We used the 2-D medium energy-flux model as in Jemberie and Langston (2005). A least-square procedure is used to invert for Q_I and Q_S using a normalized (by the square root of I_d) form of equation (1). Details of the procedure can be found in the references listed above.

In the single scattering model of Aki (1969), coda amplitude is given by,

$$A_c(\omega, t) = \frac{C e^{-\omega t/2Q_c}}{\sqrt{t}}, \qquad (2)$$

where $A_c(\omega, t)$ is the envelope of coda amplitude, Q_c the coda Q parameter, ω is angular frequency in rad/sec, and t is the time from the event origin. C is a constant that contains the source spectrum and density of scatterers.

Coda is more pronounced in the acceleration data than velocity or displacement (Figure 3) since the displacement, velocity, and acceleration fields contain progressively higher frequency waves that scatter more with distance. The acceleration envelope seismograms from blast 1 recorded by the strong motion array are shown in Figure (4). The similarity of the coda envelopes suggests using any one of them. The vertical component acceleration seismogram from the farthest strong motion station is cut between 0 and 5sec to get the P-wave and its coda, and between 5 and 30 sec to get the multimode Rayleigh-wave and its coda. A 2-pole Butterworth band-pass filter around a center frequency is applied to each of them. The center frequencies are 0.5, 1.0, 3.0, 5.0, and 10.0Hz. The lower and upper corner frequencies of the band pass filter are about 30% less and greater than the center frequency, respectively. For example, for a center frequency of 1Hz, the corner frequencies are 0.7 and 1.3, etc.

Figure (5) shows the process of determining the normalizing factor Id in Equation (1). The seismogram is band pass filtered around a center frequency, the primary arrival (P- or Rayleigh- wave) is cut, squared, integrated and the square root of the integral is Id. The envelope of the coda is computed from the filtered and normalized (with respect to Id) seismogram by calculating the amplitude of the analytical signal (Farnbach, 1975). The logarithm of the normalized equation (1 or 2) was then fit to the logarithm of the P- or Rayleigh-wave coda envelope using a least-square algorithm. Figure (6) shows plots of the envelope of the observed vertical component P-wave and its coda, and the theoretical envelope amplitude computed using the Energy Flux model. The early coda is mostly composed of near site reverberations (Jemberie and Langston, 2005) and therefore the late coda is used for the determinations of Q values.

Figures 7 (a and b) display plots of intrinsic and scattering Q values with 1-standard deviation error bars, respectively, as a function of frequency, obtained from the P-wave late coda at center frequencies of 0.5, 1, 3, 5, and 10 Hz , using the Energy Flux model. Both Q_I and Q_S increase with frequency. The Q_I values start with a value of 2.3 at 0.5Hz and increase to 48 at 10Hz. The Q_S values increase from 13 at 0.5Hz to 67 at 10Hz. There is anomalously high Q_S value (109) at 5Hz. Figure 7(c) is coda Q (Q_C) as a function of frequency obtained from the P-wave late coda using the Single Scattering model. The values of Q_C are very close to the values of Q_I. Figure 7(d) shows how good Q_I values correlate with Q_S values. Figures 8 (a and b) display Q_I and Q_S values as a function of frequency obtained from the Rayleigh-wave late coda using the Energy Flux model. Both Q values increase with frequency. The Q_I values increase from 8 at 0.5Hz to 44 at 5Hz. It dramatically increases to 225 at 10Hz. The Q_S values start from 0.9 at 0.5 Hz, increase to 30 at 1Hz, drop to 20 at 5Hz and dramatically increase to 109 at 10Hz. Figure 8(c) shows coda Q (Q_C) values as a function of frequency obtained from Rayleigh-wave late coda using the Single Scattering model. These Q_C values are close to the Q_I values as in the Rayleigh-wave late coda. In Figure 8(d) we can see a good correlation between Q_I and Q_S values.

Figure 9(a) shows comparisons between Q values from the P-wave late coda (Q_I) of the strong motion data and the P-wave (Q_P) of the weak motion data (Langston et al., 2005). The average value of Q_P is about 200 (Langston et al., 2005), while Q_I values range from a single digit to a maximum near 50. Figure 9 (b) shows comparison between

Q values from the Rayleigh-wave late coda (Q_I) of the strong motion data and the Rayleigh wave (Q_R) of the weak motion data. Q_I is less by more than 200 at 0.5Hz and by more than 50 at 3.0Hz compared to Q_R values. We interpreted the low Q-values from the strong motion data as amplitude reduction due to non-linear response of the Mississippi embayment sedimentary structure to the strong ground motion.

Resonance frequency Shift and amplitude reduction

Radial component strong-motion seismograms from blast 1 have strong coda between 16 and 22 sec that we do not see in the vertical component (Figure 2a and b). Following Langston et al.'s (2006) phases identification, the radial seismogram from the farthest strong motion station was divided in to PS-wave (0 - 4sec), higher-mode Rayleigh-wave (5-10 sec), fundamental-mode Rayleigh-wave (10 – 16 sec), and coda (16 – 22sec). The Fourier transform of each part of the seismogram is computed using the Seismic Analysis Code (SAC). The spectral amplitudes for the Rayleigh-waves and the coda are plotted together in linear-linear scale to compare the spectral peaks (Figure 10). The PS-wave spectral amplitude is too small to compare with the Rayleigh-wave and coda amplitudes.

The peak spectral amplitude shifts to lower frequencies progressively (blue to red and to green) from the coda to the fundamental mode Rayleigh-wave, and then to the higher mode Rayleigh-wave. This is a signature of non-linear response of sites under the stations during strong ground motion (Beresnev et al., 1994). Frankel et al. (2002) observed similar resonance frequency shifts of the early arrivals compared to the late

arrivals of strong motion seismograms from the M 6.8 Nisqually, Washington, earthquake.

The Fourier transforms of vertical and transverse seismograms from both strong-motion and weak motion instruments of blast 1 were also computed. Station HBAR is the closest broadband station with available data, located at 13.4km from blast 1 (Figure 1). In Figure 11,(a) the maximum amplitude of the strong motion data is about 0.2 g, and (b) the weak motion data has a maximum amplitude of about 0.0015g. Spectral ratios of transverse to vertical components for both strong and weak motion data were calculated. Figure 12 shows spectral ratio from the farthest (at 2.65228 km) strong motion station of blast 1 and from broadband station HBAR. We can see a degradation in the spectral ratio for the strong motion data compared to that of the weak motion data for frequencies less than about 6 Hz. Above this frequency, however, the strong-motion ratio is dominant over the weak-motion ratio. This is also a signature of non-linear site response during strong ground motion (Frankel et al., 2002). The radial to vertical spectral ratios (Figure 13) do not show significant differences at all frequencies for the weak and strong motion data.

Conclusions

The strong motion data from blast 1 of the ESEE show non-linear site response signatures as seen in other places from large earthquakes such as the M6.8 Nisqually, Washington, earthquake (Frankel et al., 2002). Intrinsic and scattering Q values (Q_I and Q_S, respectively) are very low during the strong ground motion of the explosions

compared to Q values from weak motions obtained by Langston et al. (2005). A shift in the resonance peak to lower frequencies of the early part compared to the late part of the radial component strong motion seismogram is also due to non-linear site effect. We also observed reduction in transverse to vertical spectral amplitude ratio of the strong motion compared to the weak motion ratio for frequencies less than 6 Hz and a reverse relation is observed for frequencies greater than 6Hz. These results prove the use of explosion data as a proxy for earthquakes' strong motion data.

This study answers the questions stated at the beginning that: (1) Do strong ground motions from large earthquakes show similar attenuation (intrinsic and scattering) as weak motions?" The answer is no. (2) Will the damping, or intrinsic attenuation increase as predicted by nonlinear models? The answer is yes. (3) Are the attenuation values from weak motions transportable to estimations of amplitudes from strong ground motions? The answer is no.

Acknowledgements

This research was supported by the U.S. Geological Survey (USGS), Department of the Interior, under the award number USGS (07HQGR0054). The author wishes to thanks Prof. Chuck Langston, of the Center for Earthquake Research and Information at the University of Memphis, for providing the explosion data and his invaluable comments. Many thanks to Prof. Solomon Bililign for encouraging the author to submit the proposal to the USGS and hosting him for one academic year at the department of Physics, North Carolina A&T State University.

References

Aki, K. (1969). Analysis of the Seismic Coda of Local Earthquakes as Scattered Waves, *J. Geophys. Res.* **74**, 615-631.

Aki, K., and B. Chouet (1975). Origin of Coda Waves: Source, Attenuation, and Scattering Effetcs, *J. Geophys. Res.* **80**, 3322-3342.

Beresnev I., K.-L. Wen, and Y. T. Yeh. (1994). Seismological evidence for nonlinear elastic ground behavior during large earthquakes, *Soil Dynamics and Engineering* 14, 103-114.

Farnbach, J.S. (1975). The Complex Envelope in Seismic Signal Analysis, *Bull. Seism. Soc. Am.* **65**, 951-962.

Field, E. H., Y. Zeng, P. A. Johnson, and I. A. Beresnev. (1998). Nonlinear sediment response during the 1994 Northridge earthquake: Observations and finite source simulations, *J. Geophys. Res.*, 103, 26869-26883.

Frankel, A., and L. Wennerberg. (1987). Energy-flux model of seismic coda: Separation of scattering and intrinsic attenuation, *Bull. Seism. Soc. Am.* 77, 1223-1251.

Frankel, A., D. L. Carver, and R. A. Williams (2002). Nonlinear ad Linear Site Response and Basin Effects in Seattle for the M 6.8 Nisqually, Washington, Earthquake, *Bull. Seism. Soc. Am.* 92, 2090-2109.

Guyer R. A., J. A. TenCate, and P. A. Johnson (1999). Hysteresis and the Dynamic Elasticity of Consolidated Granular Materials. *Physical Review Letters*, 82, 3280-3283.

Hardin, B.O., and V. P. Drnevich (1972). Shear modulus and damping in soil: design equations and curves, *J. Soil Mech. Foundations Div. ASCE*, 1972, 98, 667-92.

Jemberie, A. L., and C. A. Langston. (2005). Site amplification, scattering, and intrinsic attenuation in the Mississippi Embayment from coda waves, *Bull. Seism. Soc. Am.* 95, 1716-1730.

Johnson, P. A., A. Sutin (2005). Slow dynamics and anomalous nonlinear fast dynamics in diverse solids, *J. Acoust. Soc. Am.*, 117, 124-130.

Johnson, P. A., and P. N. J. Raolofosaon (1996). Manifestation of nonlinear elasticity in rock: Convincing evidence over large frequency and strain intervals from laboratory studies, *Nonlinear Processes in Geophysics*, 3, 77-88.

Johnson, P.A., B. Zinszner, and P. N. J. Rasolofosaon (1996). Resonance and nonlinear elastic phenomena in rock, *J. Geophys. Res. 101*, 11553-11564

Langston, C. A., P. Bodin, C. Powell, M. Withers, S. Horton, and W. Mooney. (2006). Explosion Source Strong Motions in the Mississippi Embayment, *Bull. Seism. Soc. Am.* 96, 1038-1054.

Langston, C. A., P. Bodin, C. Powell, M. Withers, S. Horton, and W. Mooney. (2005). Bulk Sediment Q_P and Q_S in the Mississippi Embayment, Central United States, *Bull. Seism. Soc. Am.* 95, 2162-2179.

Langston, C. A., W. Mooney, P. Bodin, C. Powell, and M. Withers. (2002). Experiment in New Madrid Zone to employ active source, *EOS, Trans.* AGU, 83, 473.

Langston, C.A. (1989a). Scattering of Teleseismic Body Waves Under Pasadena, California, *J. Geophys. Res.* **94**, 1935-1951.

Langston, C.A. (1989b). Scattering of Long-Period Rayleigh Waves in Western North America And the Interpretation of Coda Q Measurements, *Bull. Seism. Soc. Am.* **79**, 774-789.

Ostrovsky, L. and P. Johnson (2001). Dynamic nonlinear elasticity in geomaterials, *Rivista del Nuovo Cimento* 24, 1-46.

Schneider, J., A., L. Hoyos Jr., P. W. Mayne, E. J. Macari, and G. J. Rix. (1999). Field and laboratory measurements of dynamic shear modulus of Piedmont residuals soils, behavioral characteristics of residual soils, *GSP* 92, ASCE, Reston, VA, 12-25.

Self, R.P. (1993). Late Tertiary to Early Quaternary Sediments in the Gulf Coastal Plain and Lower Mississippi Valley, *Southeast. Geol.* **33**, 99-110.

Stearns, R.G. (1957). Cretaceous, Paleocene, and Lower Eocene geological history of the Northern Mississippi Embayment, *Geol. Soc. Am. Bull.* 68, 1077-1100.

Stearns, R.G., and M.V. Marcher (1962). Late Cretaceous and Subsequent Structural Development of the Northern Mississippi Embayment Area, *Geol. Soc. Am. Bull.* **73**, 1387-1394.

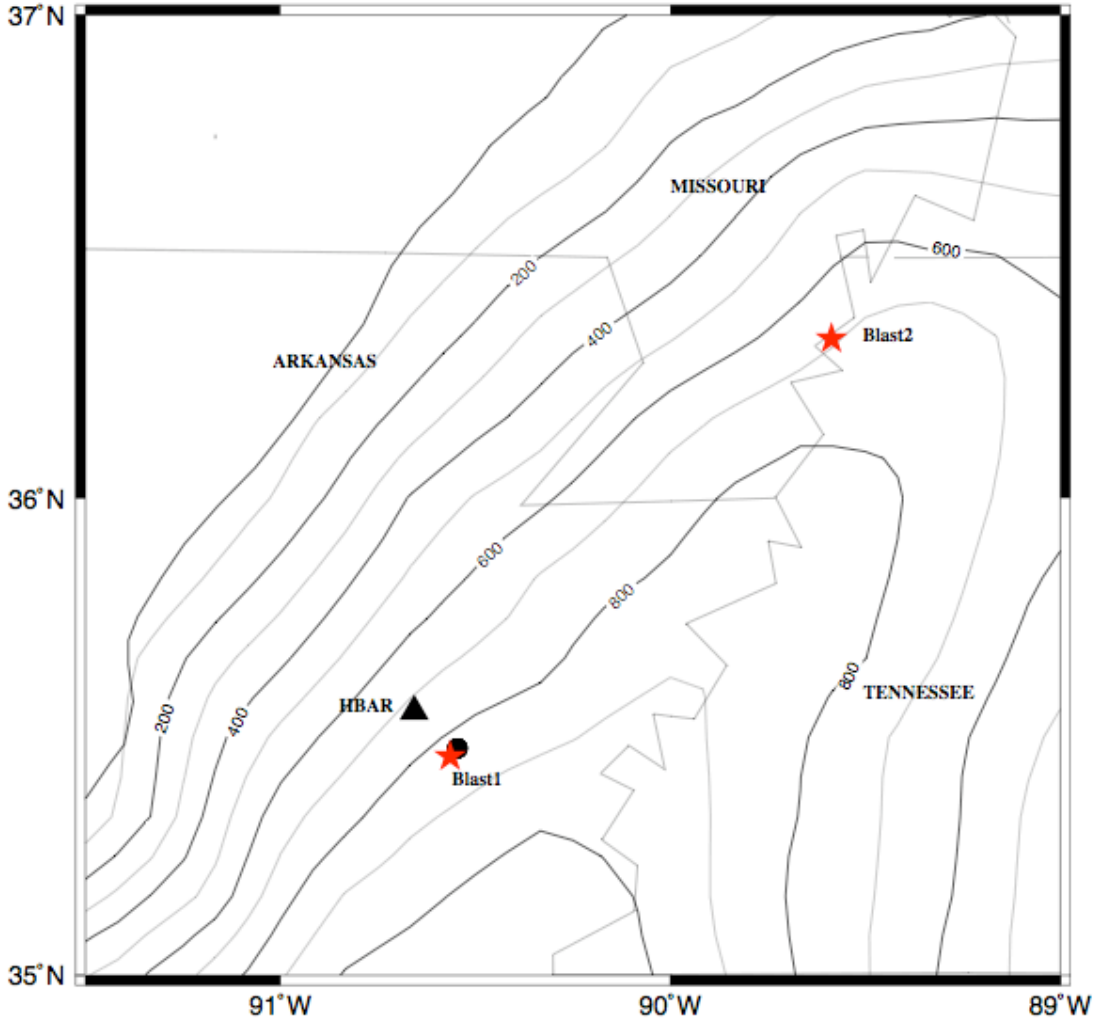

Figure 1. Part of the Mississippi embayment in Tennessee, Arkansas and Missouri of the Central United States. The annotated contours are sediment thicknesses in meters, of the embayment. The stars are the 2500 lb (Blast 1) and 500 lb (Blats 2) explosions that were detonated by the ESEE experiment on October 29, 20002 and October 30, 2002, respectively. The black filled circle is array of strong motion instruments near Blast 1. The black triangle is the closest broadband station HBAR near blast 1.

(a)

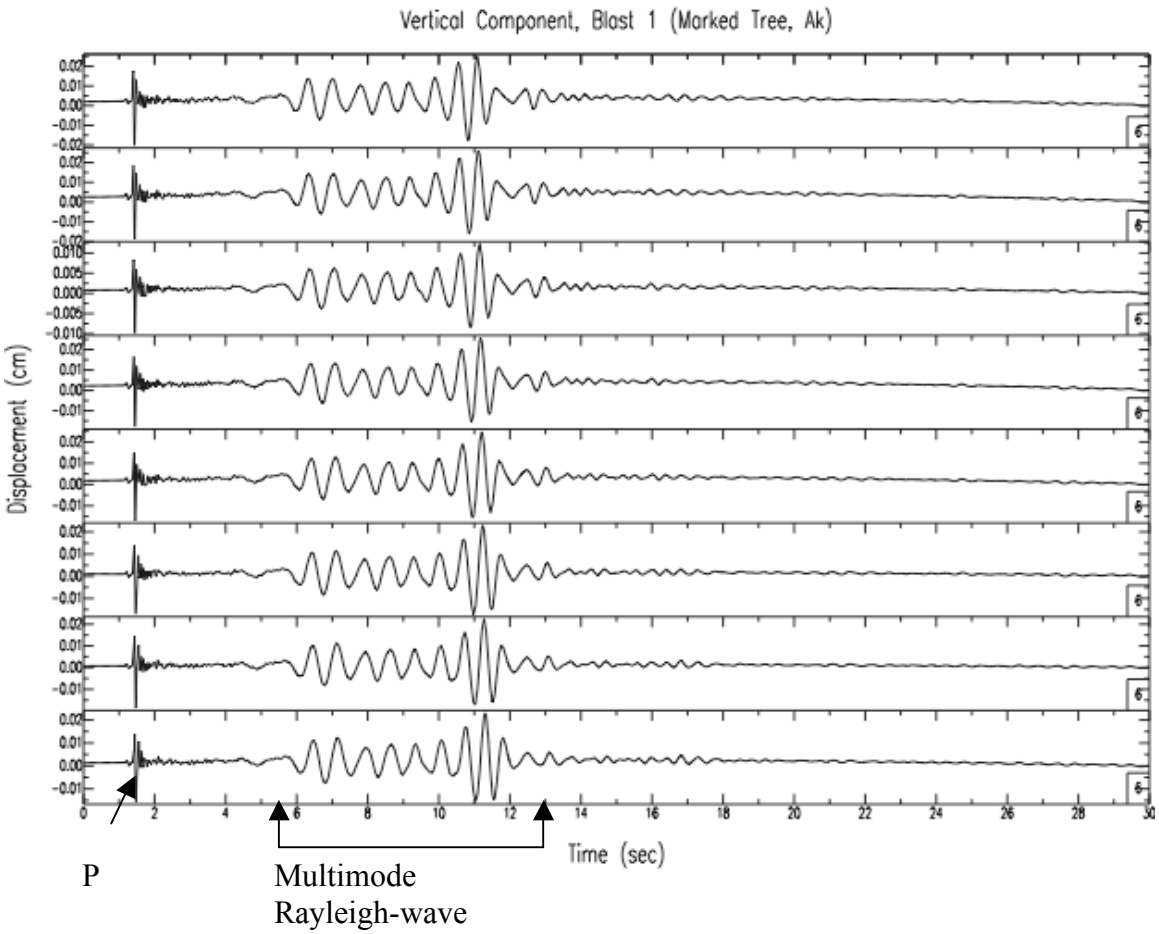
Vertical Component, Blast 1 (Marked Tree, Ak)
Displacement (cm)
Time (sec)
2.55624km
2.57029km
2.58319km
2.59724km
2.61129km
2.62457km
2.63786km
2.65228km
P
Multimode
Rayleigh-wave

(b)

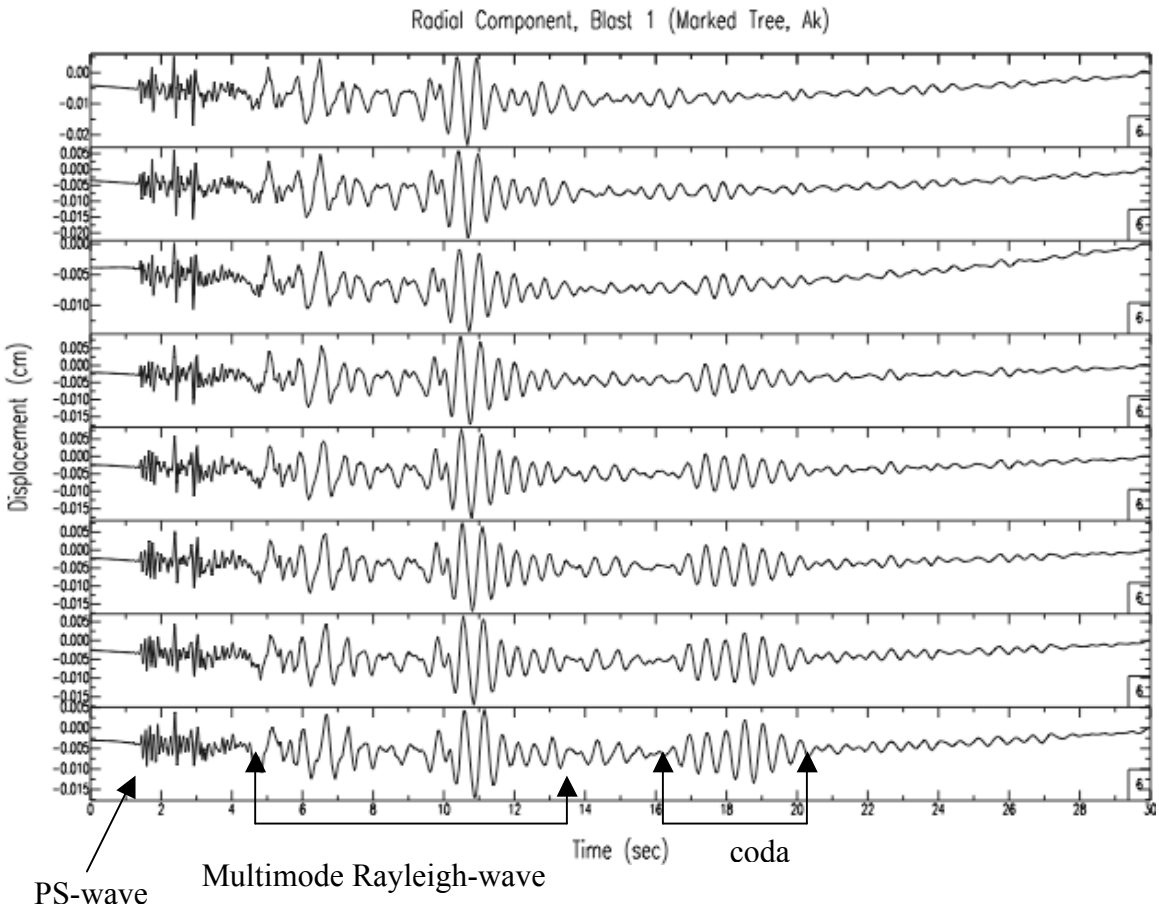
Radial Component, Blast 1 (Marked Tree, Ak)
Displacement (cm)
Time (sec)
PS-wave
Multimode Rayleigh-wave
coda

(c)

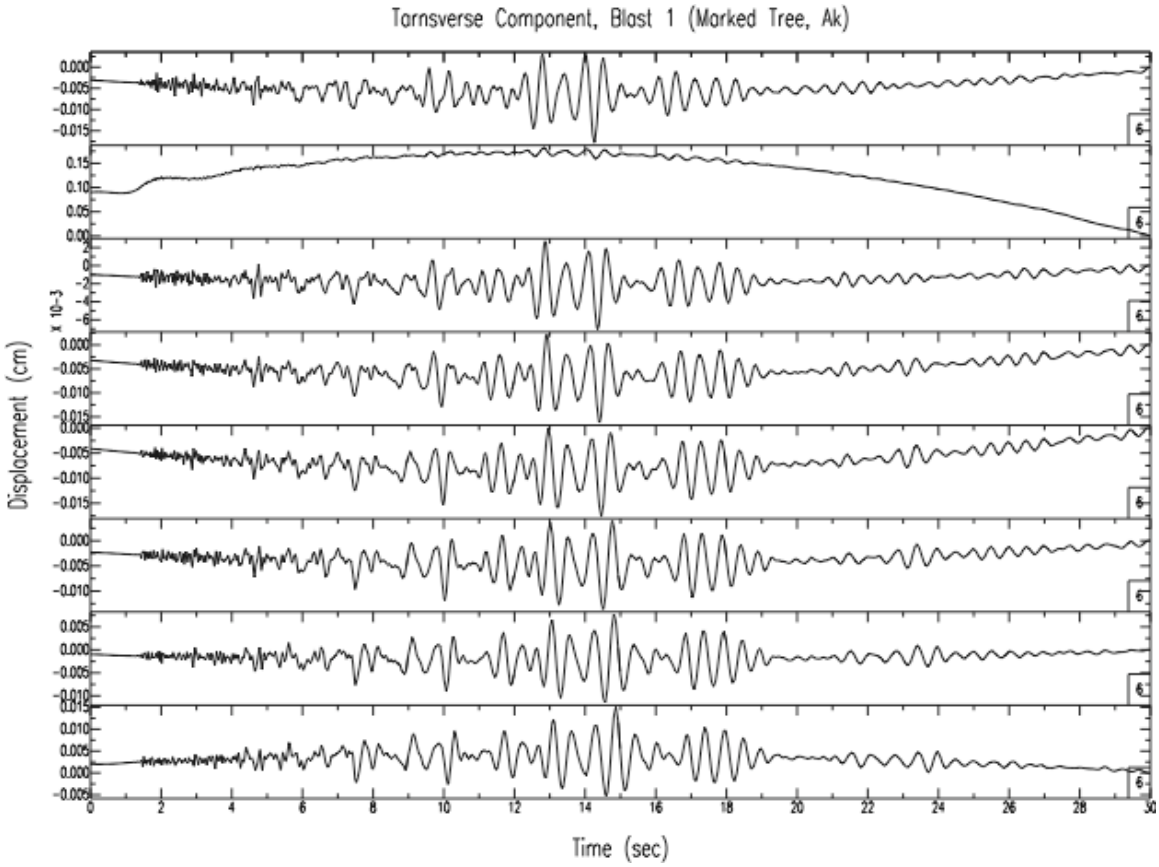

Figure 2. (a) Vertical, (b) radial, and (c) transverse component strong motion seismograms from blast 1 recorded by 8 stations, 2.55624 km to 2.65228 km away from the explosion. The phase interpretations are from Langston et al. (2006).

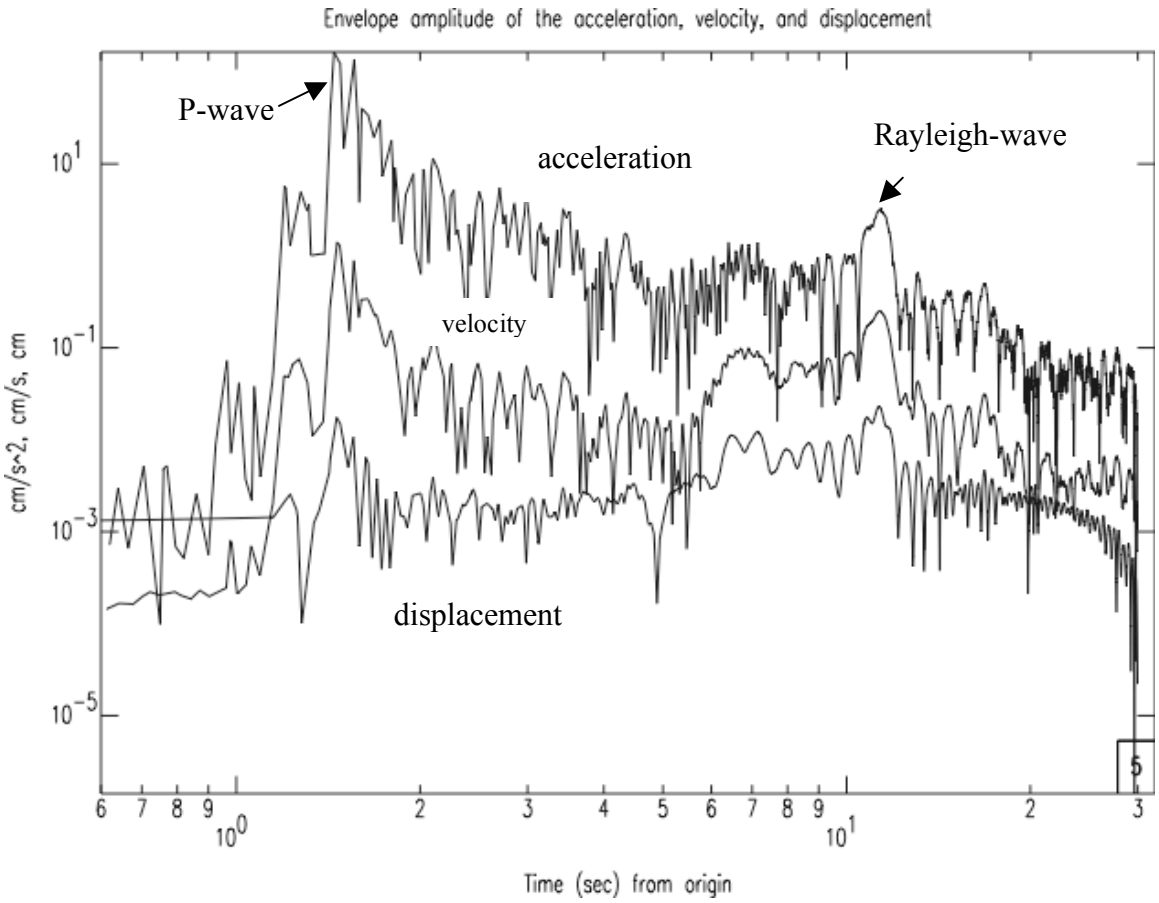

Figure 3. Envelope amplitudes of acceleration, velocity and displacement seismograms from the farthest station of the strong motion array near blast 1. The acceleration envelope has longer coda after the P-wave and the Rayleigh-wave main arrivals.

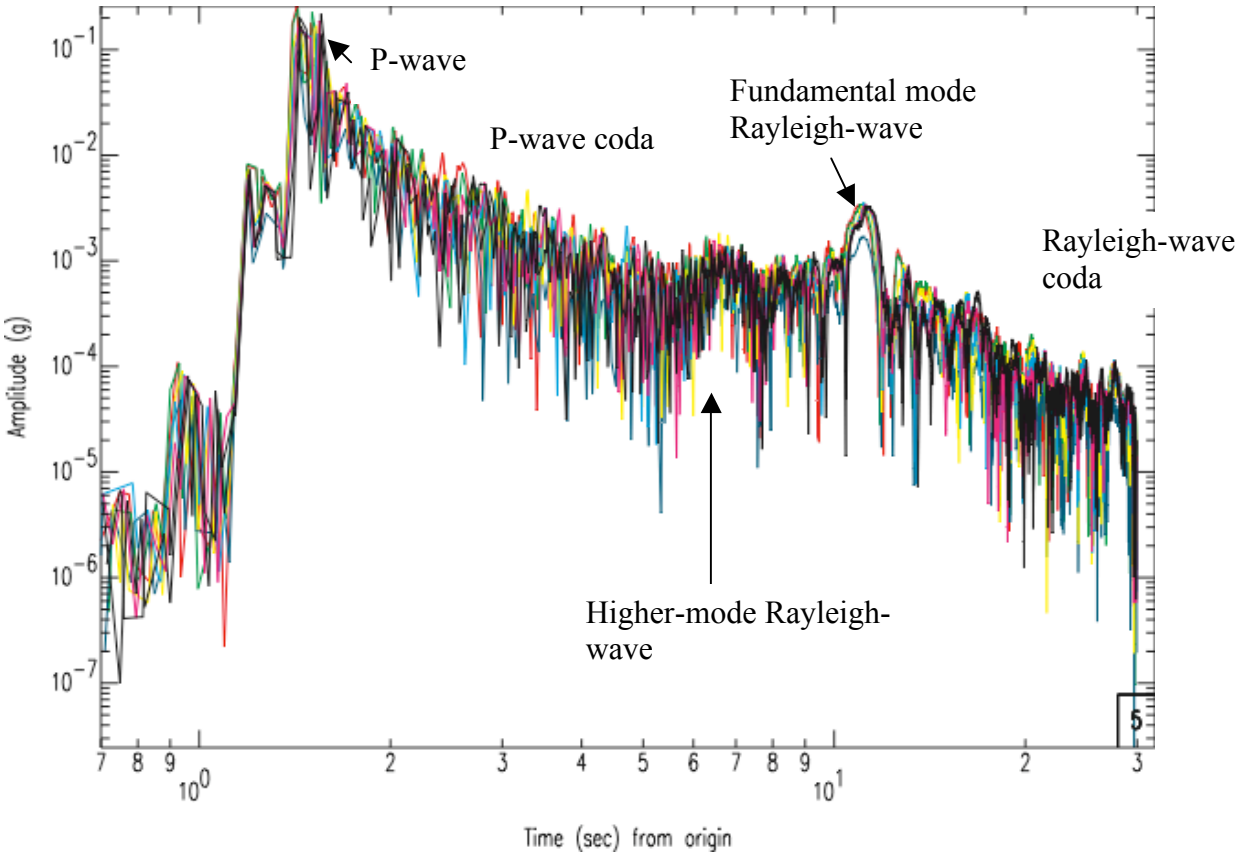

Figure (4) Vertical component acceleration envelope amplitude from all (8) of the strong motion seismographs near blast 1. Notice the similarity of the envelope amplitudes.

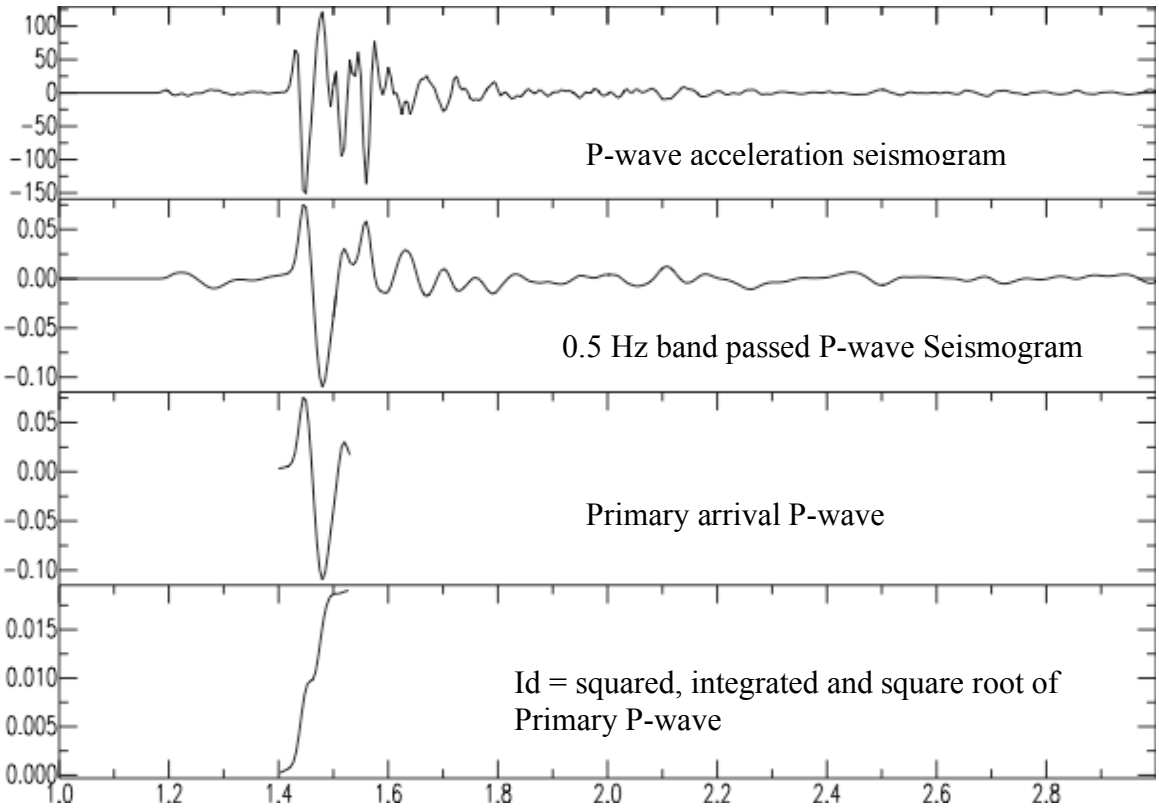

Figure 5. The process of calculating the normalization factor I_d: the P- (or Rayleigh-) wave is band passed around a center frequency (0.5Hz in this case), the primary arrival is cut, squared , integrated and the square root of the integral becomes I_d.

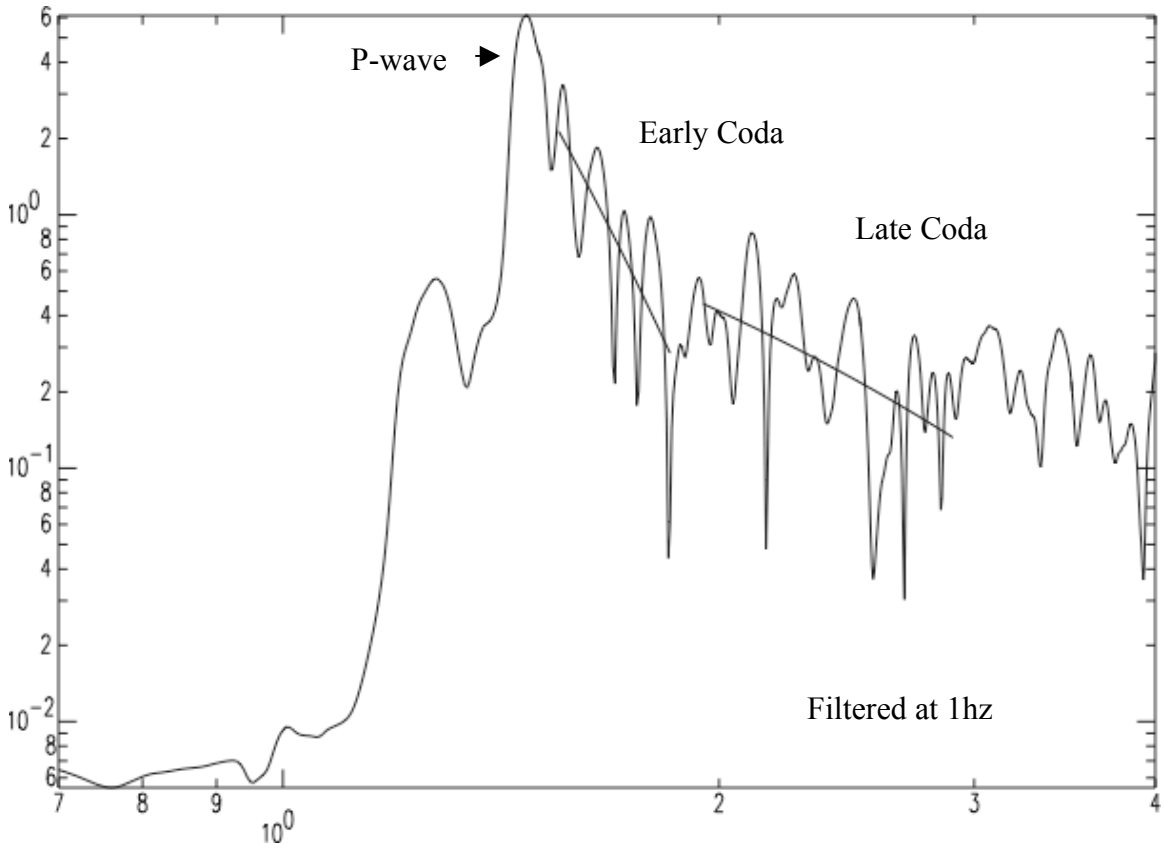

Figure 6. Envelope amplitude of the observed P-wave seismogram with its early and late coda, filtered at 1Hz, The straight lines are the theoretical envelope amplitudes, calculated using Equation 1 or 2, fit to the observed early and late coda.

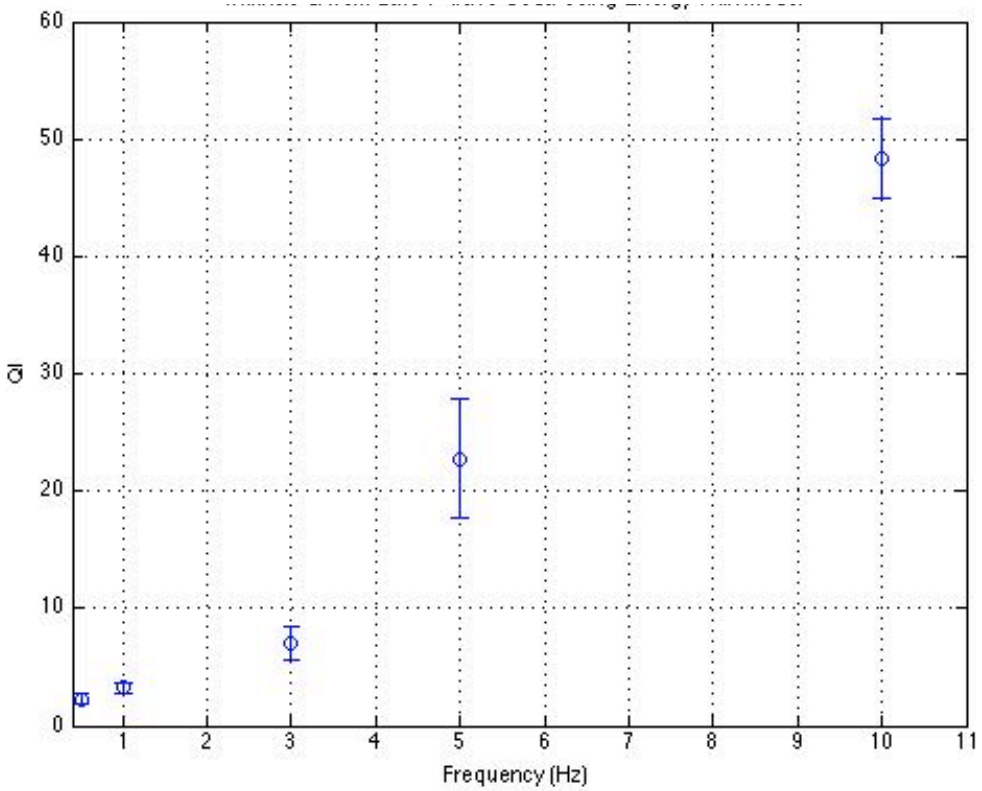
Qi
Frequency (Hz)

(a)

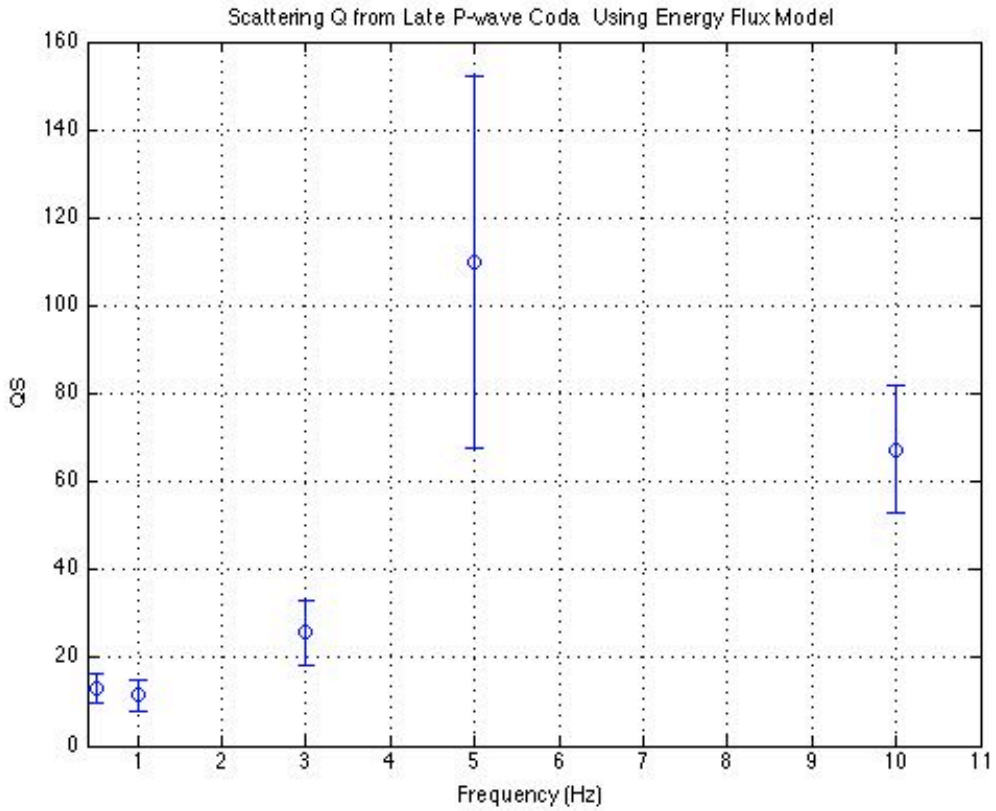
Scattering Q from Late P-wave Coda Using Energy Flux Model
QS
Frequency (Hz)

(b)

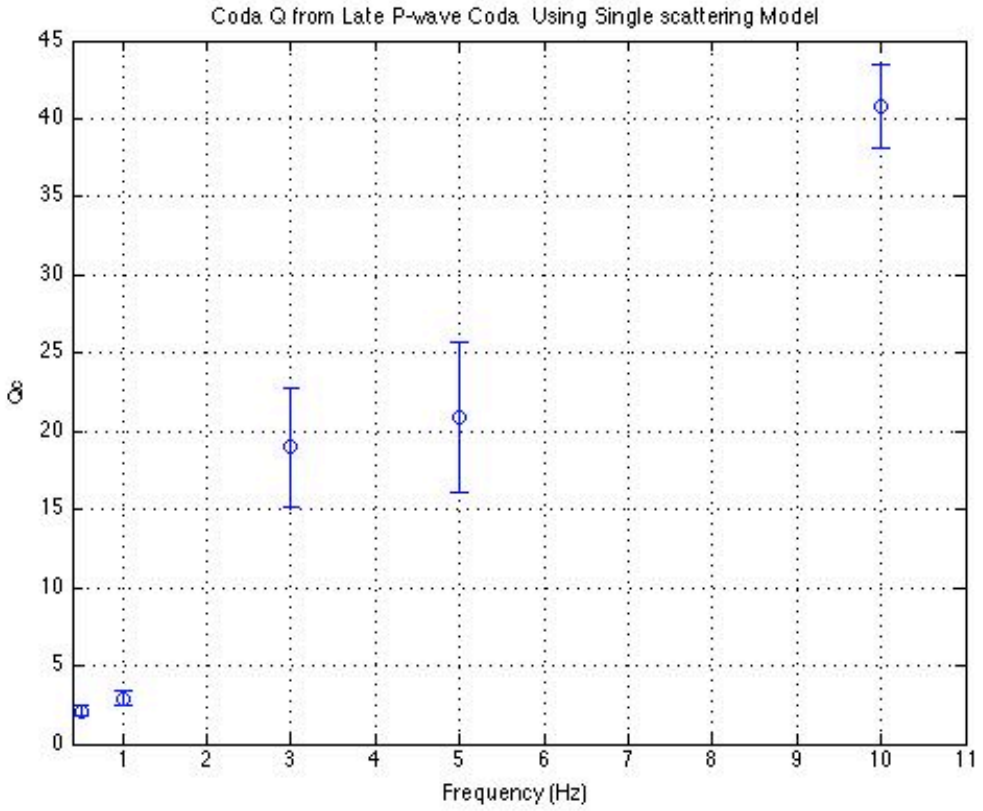
Coda Q from Late P-wave Coda Using Single scattering Model
Q
Frequency (Hz)
0
5
10
15
20
25
30
35
40
45
1
2
3
4
5
6
7
8
9
10
11

(c)

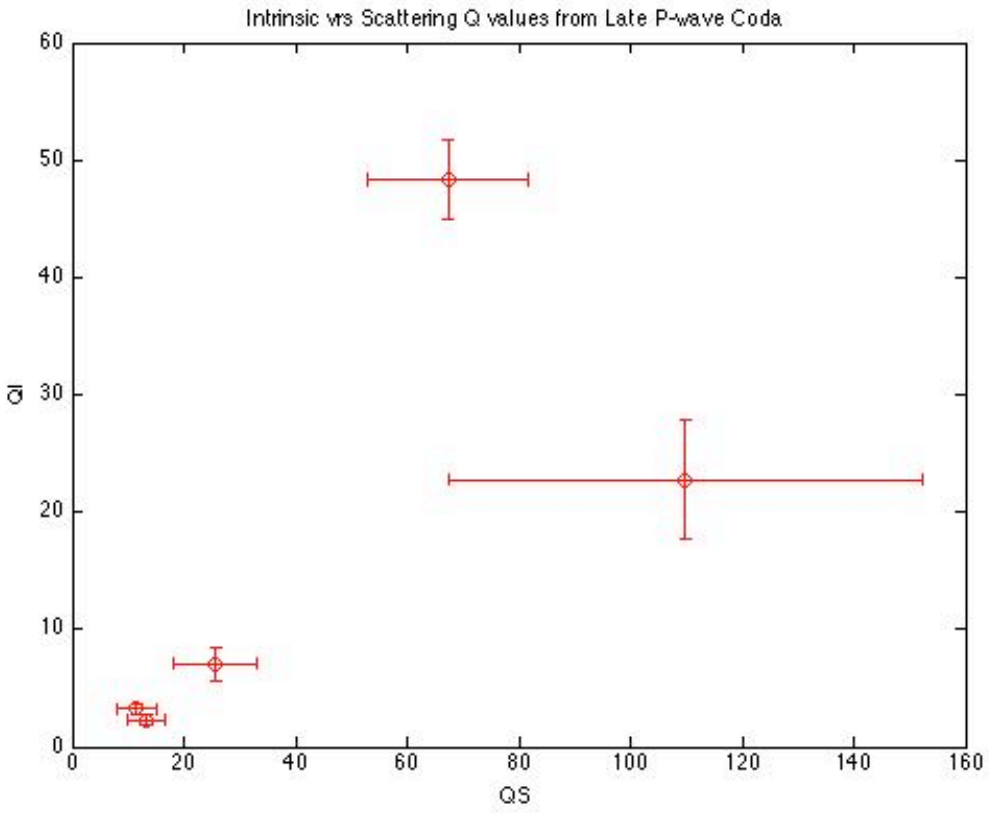

(d)

Figure 7. (a) Intrinsic Q (Q_I), (b) scattering Q (Q_S), and (c) single-scattering coda Q (Q_C) values with error bars as a function of frequency determined from the P-wave late coda of the strong motion seismograms, using the Energy Flux model (a and b) and Aki's single scattering model (c). There is a general increase of both Q_I and Qs values with frequency. Q_C increases with frequency and its values are close to the values of Q_I at each center frequency. (d) Q_I versus Q_S to show how good they are correlated.

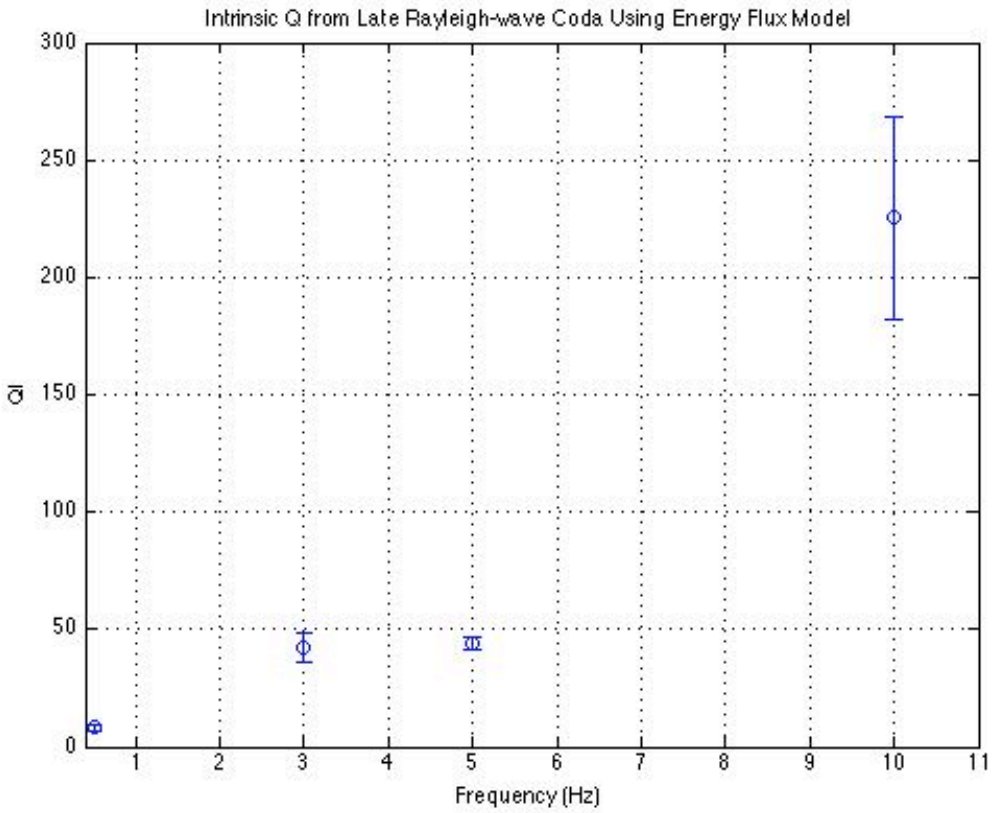
Intrinsic Q from Late Rayleigh-wave Coda Using Energy Flux Model
300
250
200
150
100
50
0
Q
1
2
3
4
5
6
7
8
9
10
11
Frequency (Hz)

(a)

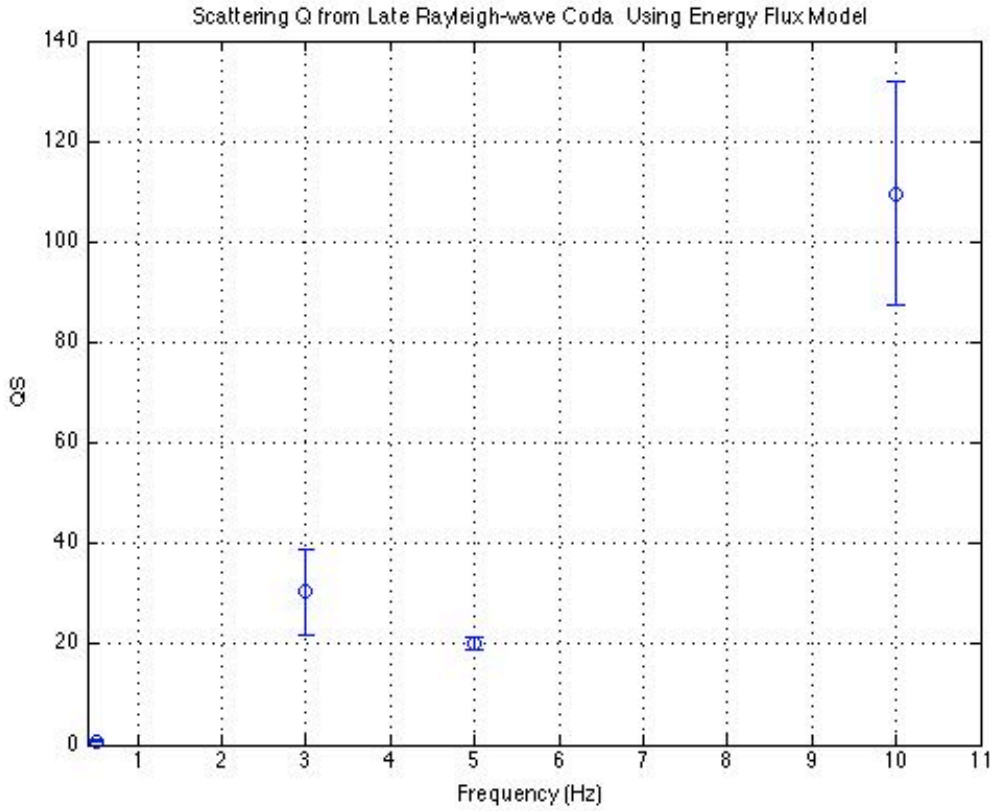
Scattering Q from Late Rayleigh-wave Coda Using Energy Flux Model
140
120
100
80
60
40
20
0
Qs
1
2
3
4
5
6
7
8
9
10
11
Frequency (Hz)

(b)

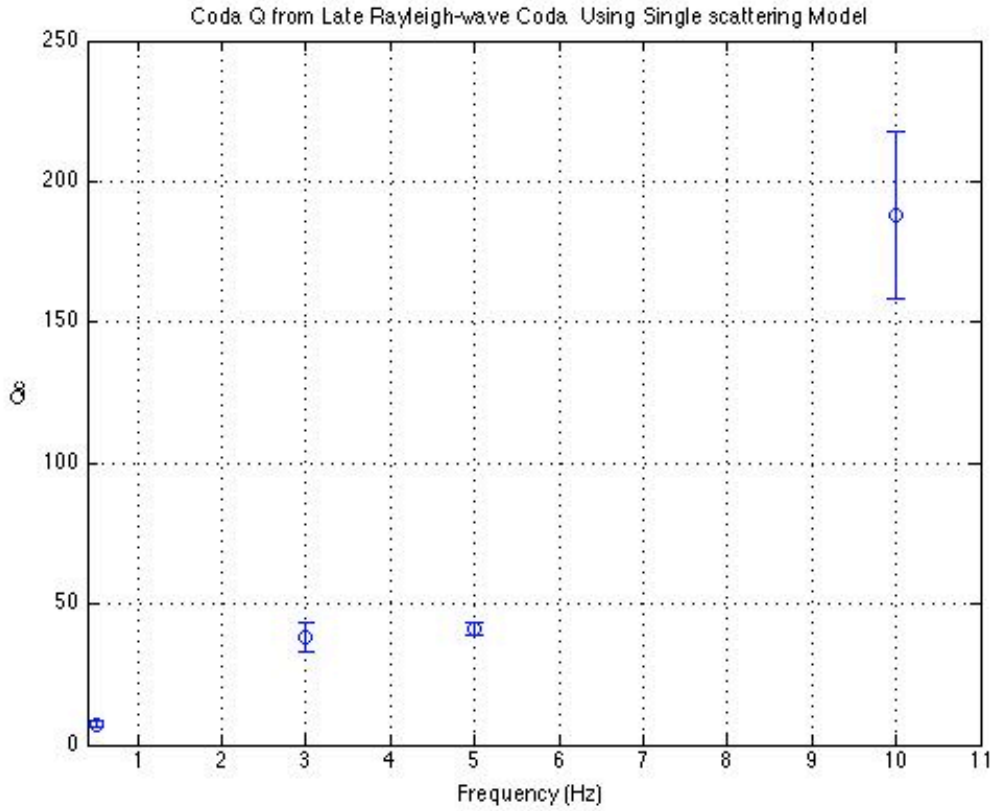
Coda Q from Late Rayleigh-wave Coda Using Single scattering Model
250
200
150
100
50
0
Q
1
2
3
4
5
6
7
8
9
10
11
Frequency (Hz)

(c)

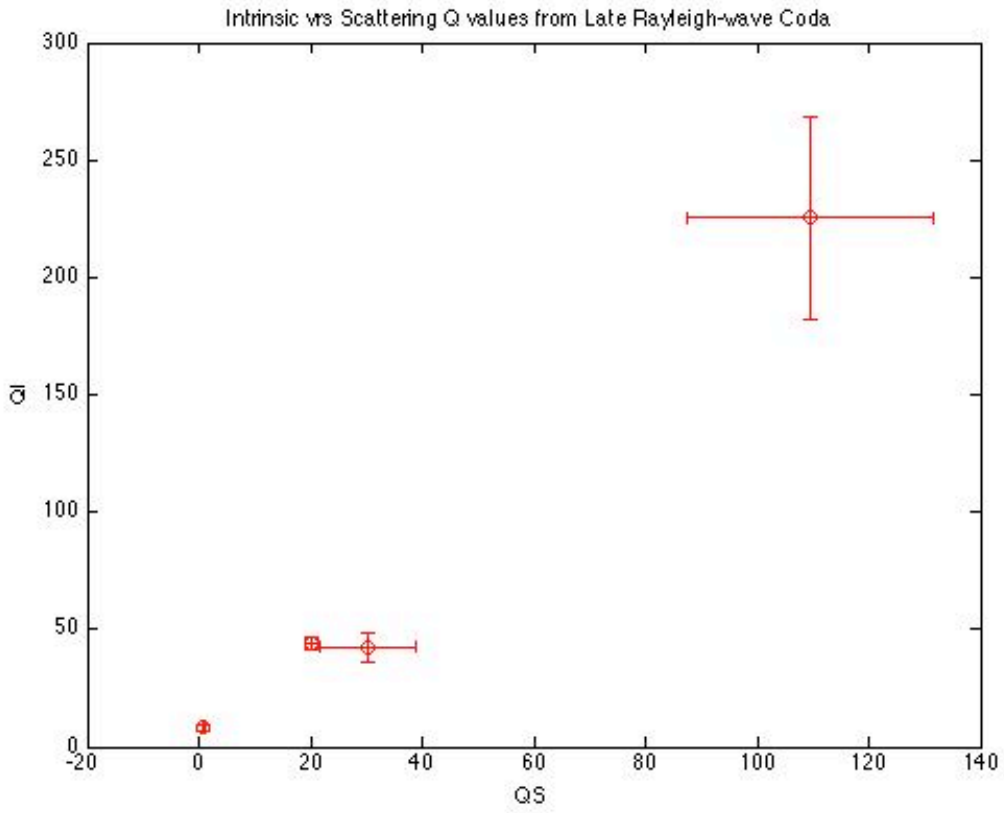

(d)

Figure 8. (a) Intrinsic Q (Q_I), (b) scattering Q (Q_S), and (c) single scattering coda Q (Q_C) values with error bars as a function of frequency determined from the fundamental mode Rayleigh-wave late coda of the strong motion seismograms, using the Energy Flux model (a and b) and Aki's single scattering model (c). There is a general increase of both Q_I and Qs values with frequency. Q_C increases with frequency and its values are close to the values of Q_I at each center frequency. (d) Q_I versus Q_S to show how good they are correlated.

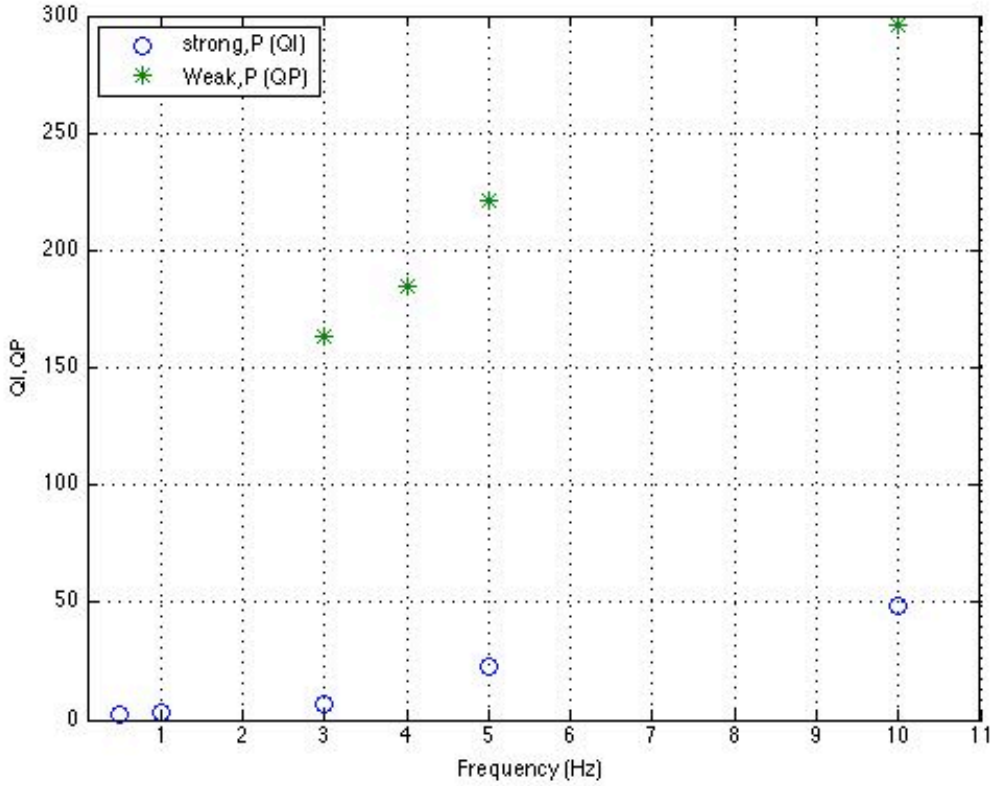
strong,P (QI)
Weak,P (QP)
QI,QP
Frequency (Hz)
0
50
100
150
200
250
300
1
2
3
4
5
6
7
8
9
10
11

(a)

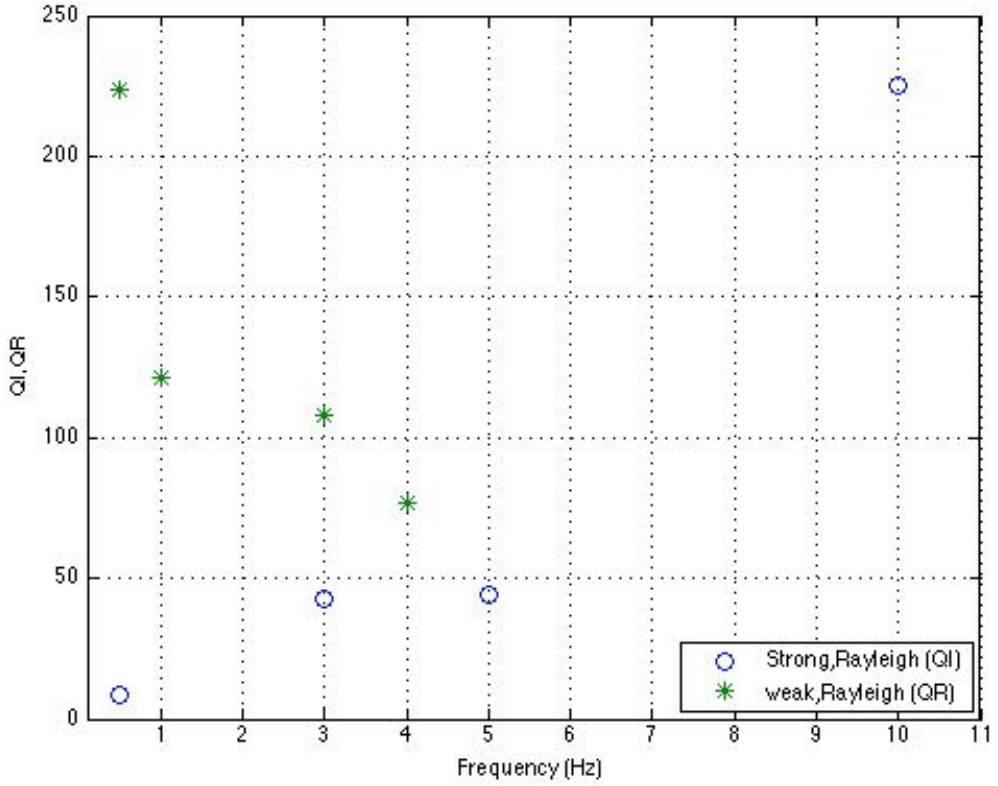
Strong,Rayleigh (QI)
weak,Rayleigh (QR)
QI,QR
Frequency (Hz)
0
50
100
150
200
250
1
2
3
4
5
6
7
8
9
10
11

(b)

Figure 9. (a) Comparison between Q values determined from strong motion P-wave coda (Q_I), this study, and weak motion P-wave Q (Q_P) , form Langston et al. (2005) . (b) Comparison between Q values from strong motion Rayligh-wave coda Q (Q_I), this study, and weak motion Rayleigh wave Q (Q_R), from Langston et al. (2005).

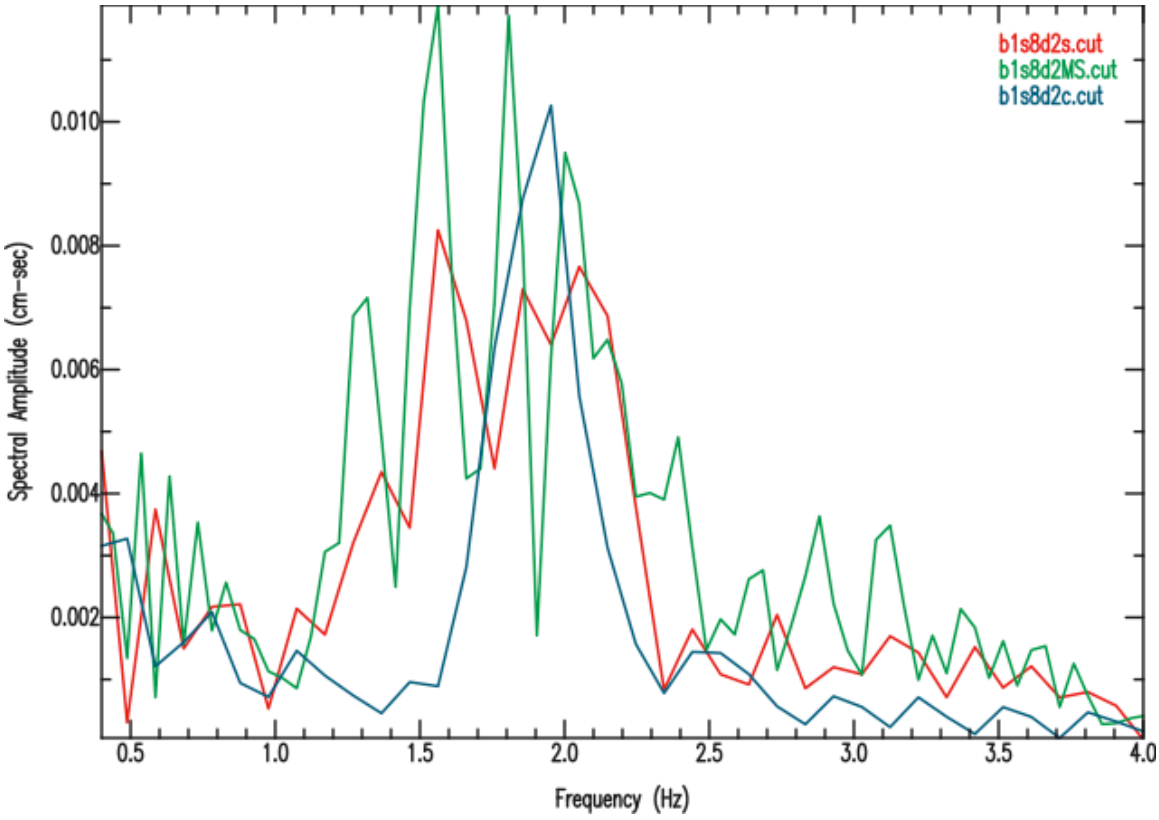

Figure 10. Spectral amplitudes of the Multimode Raleigh-wave (green), the fundamental-mode Rayleigh-wave (red) and the coda (blue) between 16and 22 sec of the radial component strong motion seismogram.

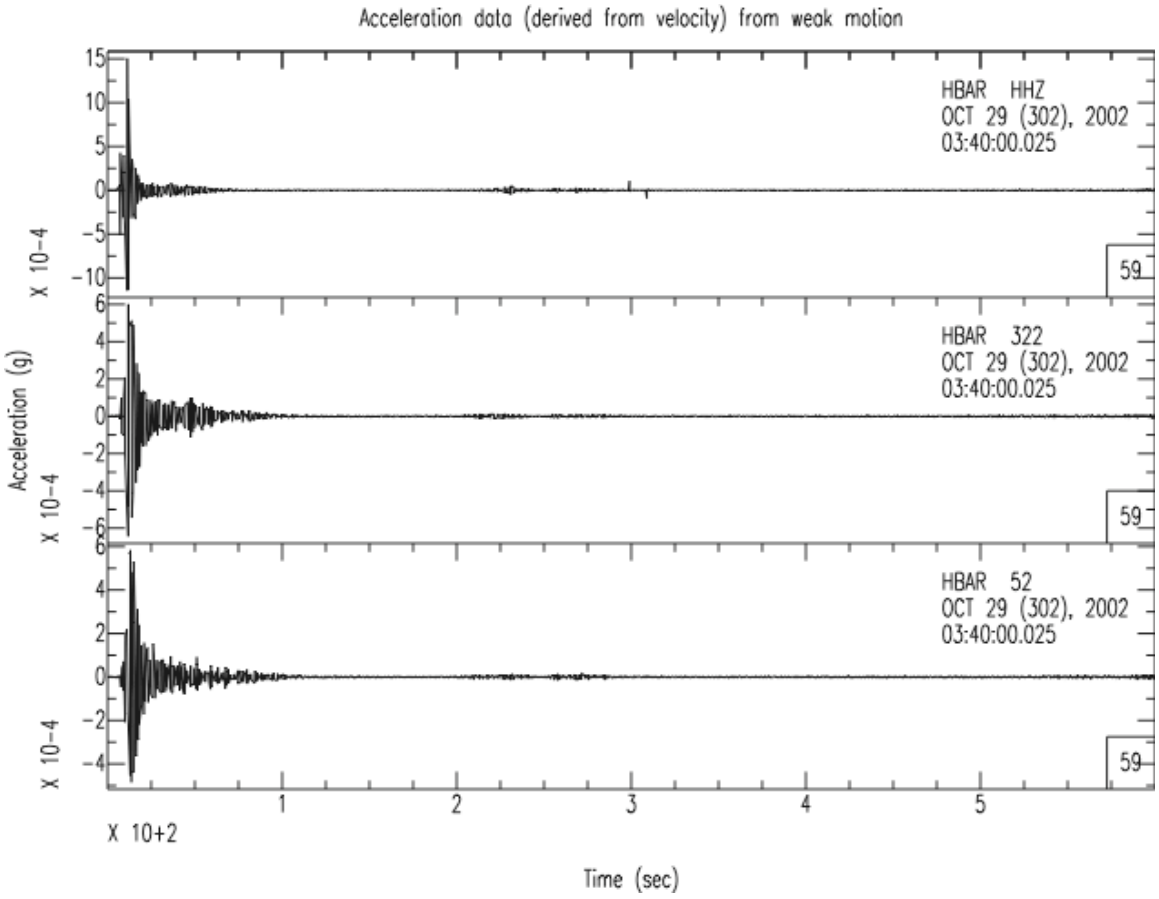
Acceleration data (derived from velocity) from weak motion
HBAR HHZ
OCT 29 (302), 2002
03:40:00.025
HBAR 322
OCT 29 (302), 2002
03:40:00.025
HBAR 52
OCT 29 (302), 2002
03:40:00.025
59
Acceleration (g)
X 10-4
X 10+2
Time (sec)

(a)

(b)

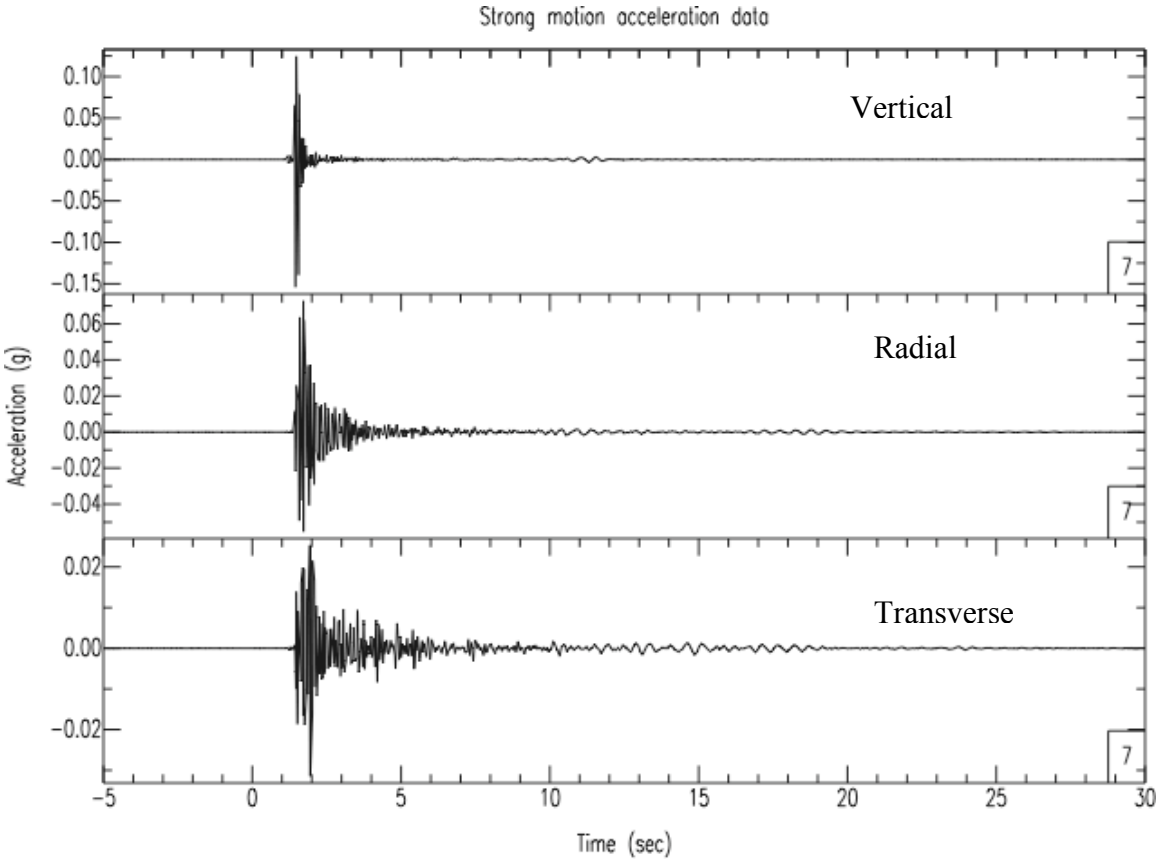

Figure 11. (a) Three component weak motion from blast 1 recorded by broad band station HBAR located about 13 km away from the explosion. (b) Three component strong motion data recorded by the farthest station in the array close to blast 1. The Amplitude in both plots is in units of g.

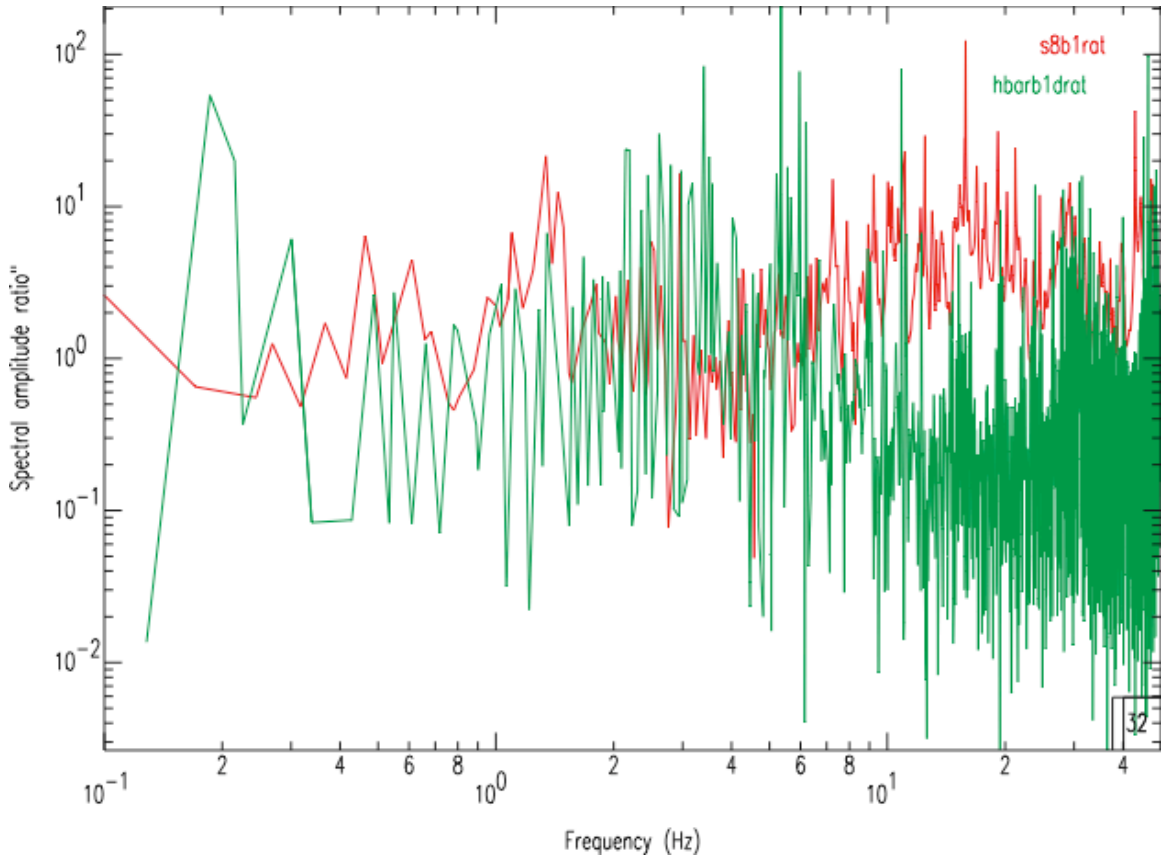

Figure 12. Spectral ratio of transverse to vertical seismograms from farthest strong-motion station (red) and weak-motion station HBAR (green).

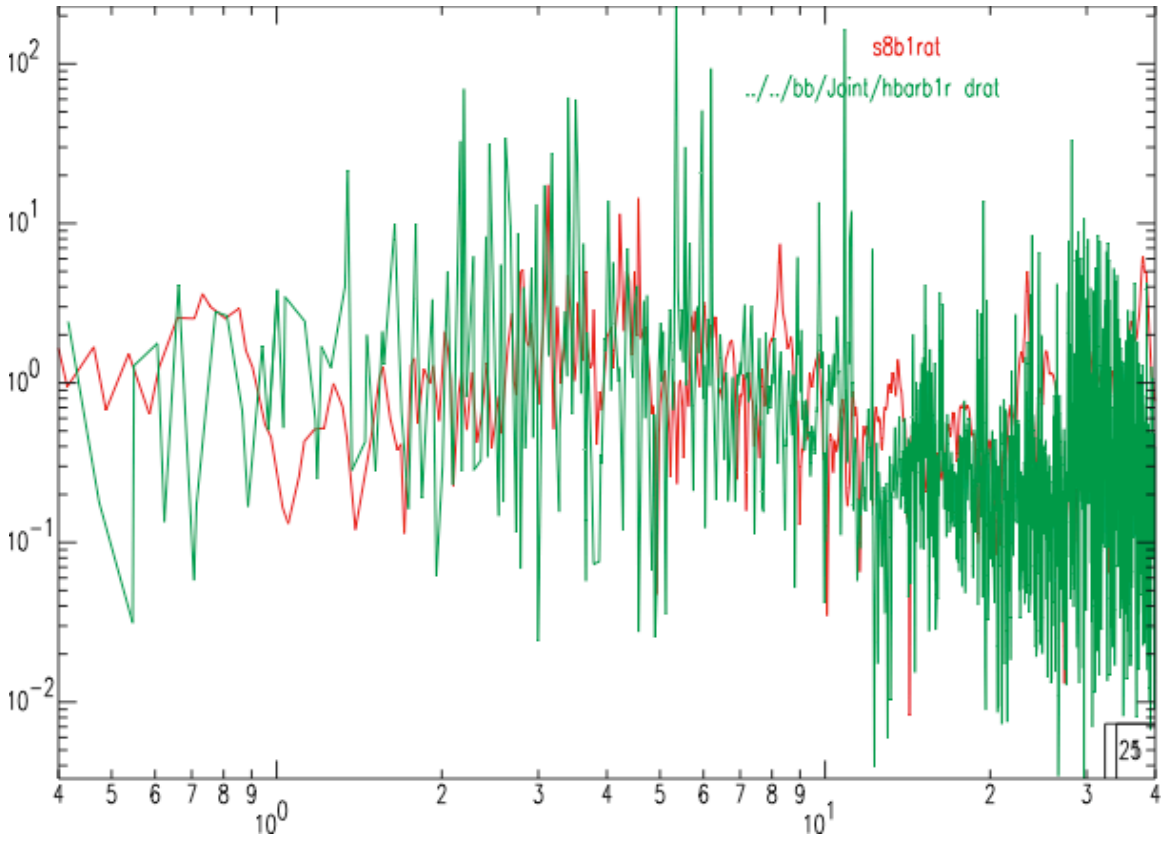

Figure 13. Spectral ration of radial to vertical seismograms from farthest strong-motion station (red) and weak-motion station HBAR (green).